

# Vectorial Growth of Metallic and Semiconducting Single-Wall Carbon Nanotubes

Ernesto Joselevich\*

*Department of Materials and Interfaces, Weizmann Institute of Science,  
Rehovot 76100, Israel*

Charles M. Lieber\*

*Department of Chemistry and Chemical Biology, Harvard University,  
Cambridge, Massachusetts 02138*

*Received June 10, 2002; Revised Manuscript Received August 13, 2002*

## ABSTRACT

A new approach for vectorial growth of single-wall carbon nanotube arrays is presented. The origin of growth is defined by patterning the catalyst nanoparticles, while the direction of growth is defined by a local electric field parallel to the substrate. Statistical analysis of the nanotube angular distribution indicates that field-directed growth can discriminate between metallic and semiconducting nanotubes during their formation. Vectorial growth could be used to produce nanotube-based circuitry for molecular electronics.

Carbon nanotubes<sup>1</sup> exhibit outstanding structural, mechanical, and electronic properties, which make them promising building blocks for molecular electronics.<sup>2,3</sup> Recently, we have presented a new approach for the realization of a highly integrated, ultrafast, nonvolatile random access memory for molecular computing based on carbon nanotubes, where the nanotubes act as both interconnect wires and functional devices,<sup>4</sup> and other groups have been exploring nanotube field-effect transistors as components for nanoelectronics.<sup>5–7</sup> To achieve the integration of large arrays of such devices, however, two critical issues must be effectively addressed. First, to produce large arrays of SWNTs on surfaces, it is necessary to develop reliable synthetic methods for the production of SWNTs in defined locations and directions. Several approaches have been reported to address this issue. SWNTs have been selectively deposited from liquid suspensions on chemically functionalized patterns,<sup>8</sup> or using microfluidics and electric fields.<sup>9</sup> The success of this approach for the assembly of isolated SWNTs has been limited due to the tendency of SWNTs to aggregate into ropes and tangles. Suspended nanotube networks have been produced by chemical vapor deposition (CVD) from microfabricated pillars,<sup>10–12</sup> where directionality was attributed to a mechanism of selective pinning of the growing nanotubes on the tops of nearest neighbor pillars. Recently, directional growth of suspended SWNTs was further enhanced using electric fields.<sup>13</sup> SWNTs have also been found to grow on well-

defined silicon surfaces in four or six possible directions that are defined by the lattice of Si(100) or Si(111) substrates, respectively.<sup>14</sup>

A second critical issue for the application of carbon nanotubes as building blocks in molecular electronics is the need to organize selectively metallic or semiconducting nanotubes, since semiconductors and metals play very different roles in electronic circuits and devices. SWNTs can be either metallic or semiconducting, depending on both their diameter and chirality. Assuming a random distribution of nanotube chiralities, one-third of the nanotubes should be metallic and two-thirds should be semiconducting. Unfortunately, no methods are yet available for the production of (or separation of heterogeneous mixtures to yield) relatively pure samples consisting of either metallic or semiconducting carbon nanotubes. Recently, a method for the selective destruction of metallic SWNTs from mixed ropes has been achieved using electrical breakdown.<sup>5</sup> Although these developments are certainly significant, both the production of ordered SWNT arrays on surfaces and the selection of metallic vs semiconducting SWNTs remain two major obstacles toward nanotube-based electronic technology.

Vectorial growth of SWNTs is a new approach whereby the growth of these one-dimensional nanostructures is defined in the form of a vector, i.e., having an origin ( $x, y$ ), a direction ( $\phi$ ), and a length ( $L$ ), as represented in Figure 1a. Ideally, one would also like to gain control over the diameter ( $d$ ) and the chirality ( $\theta$ ) of the SWNTs, which determine their electronic type, i.e., metallic or semiconducting. Our working

\* Corresponding authors. E-mail: ernesto.joselevich@weizmann.ac.il; cml@cmliris.harvard.edu.

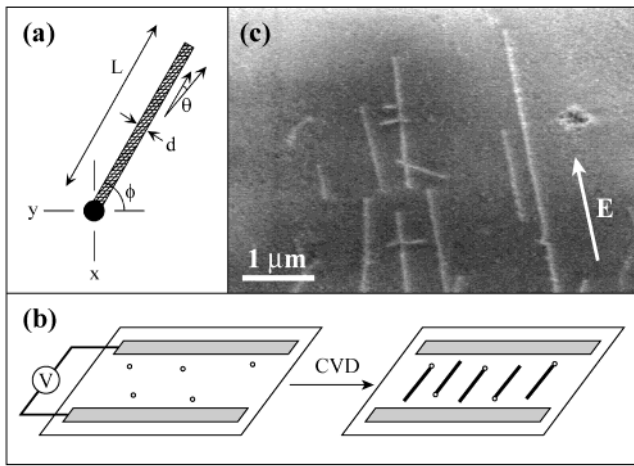


**Figure 1.** (a) Vectorial growth of a single-wall carbon nanotube (SWNT) on a surface from a well-defined catalytic particle (black dot) with ideal control over geometry and structure. Geometrical parameters: origin ( $x,y$ ), direction ( $\phi$ ), and length ( $L$ ). Structural parameters: diameter ( $d$ ) and chirality ( $\theta$ ). (b) Schematic representation of the field-directed growth of carbon nanotubes on a silicon chip containing a pair of microfabricated electrodes (in gray). Nanotubes grow catalytically from the ferrihydrite nanoparticles (3–5 nm) deposited on the surface between the electrodes. (c) SEM image of SWNT grown under an electric field of  $4 \times 10^6$  V/m parallel to the plane of the substrate. The vector  $E$  indicates the electric field, which was created by applying 100 V across the microelectrodes,  $25 \mu\text{m}$  apart. The SWNTs were grown for 10 min at  $800^\circ\text{C}$  in a 1 L/min flow of 0.2%  $\text{C}_2\text{H}_4$ , 40%  $\text{H}_2$ , and  $\sim 60\%$  Ar.

hypothesis was that the origin of the growth vector can be defined by the position of the patterned catalyst nanoparticles, and the direction of growth can be imposed by an aligning force acting on the growing nanotube. In this work, we investigate the use of an electric field as an aligning force during the growth of SWNTs by CVD on oxidized silicon wafers.<sup>15</sup> The electric field is locally created by a pair of microfabricated electrodes<sup>16</sup> on the substrate, as schematically represented in Figure 1b. When SWNTs grow between the electrodes, the electric field will induce a dipole in each growing SWNT, parallel to its principal axis, and then exert a torque on these induced dipoles, forcing the nanotubes to grow parallel to the electric field.

The geometric distribution of a typical sample of SWNTs of different lengths grown by CVD from randomly deposited ferrihydrite nanoparticles<sup>17,18</sup> (3–5 nm) is shown Figure 1c.<sup>19</sup> The nanotubes were grown in an electric field of  $4 \times 10^6$  V/m. SWNTs grown in these conditions consistently exhibit a striking distribution of orientations with respect to the electric field, which can be qualitatively described as follows. When the SWNTs are longer than ca.  $1 \mu\text{m}$ , most nanotubes are found to lie nearly parallel to the electric field. However, when the nanotubes are shorter than this critical length of ca.  $1 \mu\text{m}$ , a fraction of the nanotubes is found well oriented in the direction of the field, even if very short, while the rest of the nanotubes lie in completely random orientations.

To understand this complex angular distribution of the field-aligned nanotubes, we have considered a simple electrostatic and thermodynamic model. We assume the growing nanotubes to be free to rotate and be aligned by the electric field before they get pinned to the surface. The torque exerted

by an electric field on a polarizable cylinder, and its associated energy of rotation, are given by eqs 1 and 2,

$$T = \frac{1}{2} \alpha_{zz} L E^2 \sin 2\phi \quad (1)$$

$$U = \frac{1}{2} \alpha_{zz} L E^2 \sin^2 \phi \quad (2)$$

where  $\alpha_{zz}$  is the principal term of the polarizability tensor,  $E$  is the intensity of the electric field, and  $\phi$  is the angle between the nanotube and the field. Static polarizabilities of SWNTs have been calculated by tight-binding methods<sup>20</sup> for a series of structural indices ( $n,m$ ) and found to be inversely proportional to the square of their band gap, following eq 3, where  $m$  is the electron mass,  $A$  is the area per C atom on the graphene sheet and  $\bar{E}_g$  is an “average gap” proportional to the actual band gap of the nanotube, designated as  $E_g$ . The overall proportionality factor of  $\alpha_{zz}$  with  $R/E_g^2$  is  $17.8 \text{ eV}^2 \text{ \AA}$ . The band gap  $E_g$  is nearly zero for metallic nanotubes (except for very thin ones<sup>21</sup> where a small gap may be present), while for semiconducting nanotubes it has been found<sup>22</sup> to be  $E_g = a_{c-c} \gamma_0 / R$ , where  $a_{c-c}$  is the nearest-neighbor carbon–carbon distance, 0.142 nm, and  $\gamma_0$  is the corresponding interaction energy, 2.9 eV. Thus, eq 3 assigns finite values to the polarizabilities of semiconducting SWNT, but it diverges for metallic SWNT. Instead, the static polarizability of metallic SWNTs can be approximated by a classical electrostatic model for a continuous metallic cylinder in an electric field,<sup>23</sup> given by eq 4,

$$\alpha_{zz}^S = \left[ \frac{8\pi\hbar^2 e^2}{mA} \right] \left( \frac{R}{\bar{E}_g} \right); \quad (\bar{E}_g \approx 5.4 E_g) \quad (3)$$

$$\alpha_{zz}^M = \frac{L^2}{24 \left[ \ln \left( \frac{L}{R} \right) - 1 \right]} \left[ 1 + \frac{4/3 - \ln 2}{\ln \left( \frac{L}{R} \right) - 1} \right] \quad (4)$$

where  $L$  and  $R$  are the length and radius of the nanotube, respectively. The nanotube diameters in these samples range  $2 \pm 1$  nm, while the lengths were between 100 nm and several microns. If we consider a typical nanotube of 2 nm diameter and  $1 \mu\text{m}$  length, applying eq 3, we estimate that when the nanotube is semiconducting, its static polarizability is  $\alpha_{zz}^S = 1.1 \times 10^3 \text{ \AA}^2$ . Applying eq 4, however, we calculate that the polarizability of a metallic nanotube of similar dimensions is  $\alpha_{zz}^M = 7.8 \times 10^5 \text{ \AA}^2$ . That is, the static polarizability of the metallic nanotubes is nearly 3 orders of magnitude larger than that of the semiconducting nanotubes. We may thus expect the electric field to have a very different influence on metallic and on semiconducting nanotubes.

More significant is a calculation of the maximum energy of rotation (at  $\phi = 90$  deg), according to eq 2, compared to the thermal excitation energy at the temperature of the nanotube growth,  $800^\circ\text{C}$ , i.e.,  $kT = 0.093 \text{ eV}$ . We find that at a critical length of  $1.5 \mu\text{m}$ , a semiconducting nanotube of diameter 2 nm has a maximum energy of rotation equal to  $kT$ . However, a metallic nanotube of similar dimensions has

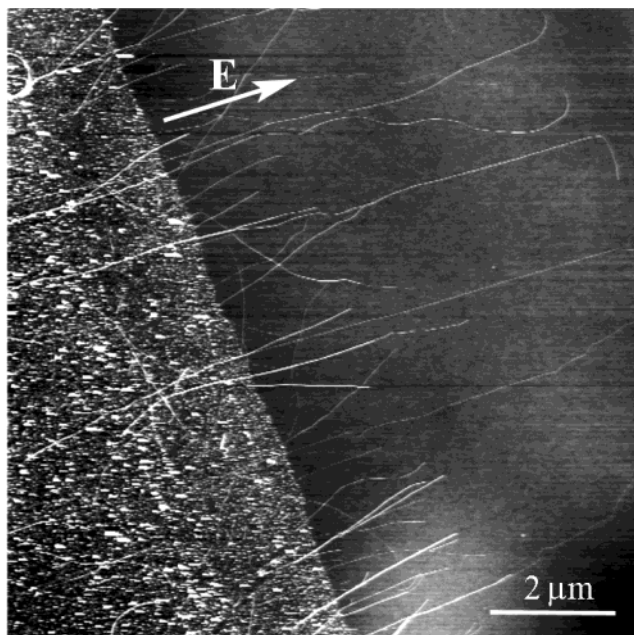


**Figure 2.** AFM image showing nonselective field-directed growth of long SWNTs from a patterned stripe of ferritin, under conditions similar to those in Figure 1.

a maximum energy of rotation of 130 eV, that is,  $1.4 \times 10^3 kT$ . Therefore, when nanotubes have lengths smaller than a micron scale, only the metallic nanotubes can be aligned by the electric field. For nanotubes longer than  $1.5 \mu\text{m}$ , however, both metallic and semiconducting nanotubes have electrostatic potentials higher than  $kT$ . Therefore, when nanotubes are longer than ca.  $1 \mu\text{m}$ , both metallic and semiconducting nanotubes have the potential to be aligned by the electric field. This prediction is in good agreement with the angular distribution observed in our samples, as shown in Figure 1c. Mechanistically, this thermodynamic control over the angular distribution of nanotubes lying on the surface indicates that growing nanotubes are indeed free to rotate and reach thermal equilibrium before they become pinned to the substrate.

The mechanisms of carbon nanotube growth<sup>15,24,25</sup> and field alignment on the substrate are not fully understood yet. However, AFM analysis<sup>26</sup> of a large number of samples produced from catalyst nanoparticles of different sizes (see Supporting Information) allows us to identify two different growth mechanisms. When the catalyst nanoparticle size is  $d = 1\text{--}2 \text{ nm}$ , very thin SWNTs ( $d = 0.8\text{--}1.4$ ) grow in wavy conformations that are not well aligned with the electric field, regardless of their length. We attribute this to a surface-bound growth mechanism. However, when the catalyst nanoparticles are  $3\text{--}5 \text{ nm}$ , SWNTs longer than  $1 \mu\text{m}$  grow straight and parallel to the electric field. It is this second mechanism that allows the nanotubes to grow upward from the substrate, with the freedom to rotate in an electric field before being pinned to the substrate. To promote this latter free growth mode, we have used ferritin<sup>25</sup> as a catalyst precursor. Upon activation, ferritin yields iron oxide cores of  $4\text{--}5 \text{ nm}$ , which are required for this growth mechanism.

Figure 2 shows a sample of long SWNTs grown in an electric field from patterned ferritin catalyst. These nano-

tubes, with a diameter dispersion of  $2.0 \pm 0.5 \text{ nm}$ , grow predominantly straight and well aligned with the electric field. As expected, nearly all of these SWNTs are oriented, because they are longer than the critical length required to align either metallic or semiconducting nanotubes in the electric field.

After having identified the different kinds of nanotubes growing on the substrate (metallic or semiconducting, free-growing or surface-growing), we can formulate a quantitative prediction for the angular distribution of metallic and semiconducting SWNTs growing on the substrate under the electric field, as given by eq 5,

$$p(\phi) = \frac{1 - p_F}{2\pi} + p_F p_M N_M \exp\left(-\frac{\alpha_{zz}^M L E^2 \sin^2 \phi}{2kT}\right) + p_F (1 - p_M) N_S \exp\left(-\frac{\alpha_{zz}^S L E^2 \sin^2 \phi}{2kT}\right) \quad (5)$$

where  $p(\phi)$  is the angular distribution,  $p_F$  is the probability of free growth,  $p_M$  is the probability of growing a metallic nanotube, and  $N_M$  and  $N_S$  are two normalization factors. The first term represents the random distribution of surface-growing nanotubes of any electronic type, the second term represents the Boltzmann distribution for the metallic SWNTs, and the third term represents a different Boltzmann distribution for the semiconducting nanotubes.

A sample of SWNTs grown in similar conditions as in Figure 2, but for a shorter time leading to nanotube lengths below  $1 \mu\text{m}$  and a field of  $2 \times 10^6 \text{ V/m}$ , is shown in Figure 3a. The lengths of these nanotubes range  $200\text{--}800 \text{ nm}$ , with a diameter dispersion of  $2.0 \pm 0.5 \text{ nm}$ . The predicted critical length for these nanotubes at this field intensity is ca.  $6 \mu\text{m}$ . In this length regime, only the metallic SWNTs should be aligned. The angular distribution, represented by the histogram in Figure 3b, shows a maximum in the direction of the electric field and can be fit with a Gaussian plus a constant. This distribution follows from eq 5, because in the case of short nanotubes and small angles it can be approximated to eq 6.

$$p(\phi) \approx \frac{1 - p_F p_M}{2\pi} + p_F p_M \exp\left(-\frac{\alpha_{zz}^M L E^2 \phi^2}{2kT}\right) \quad (6)$$

The area between the Gaussian and the constant, which can be attributed to the metallic nanotubes, is 21% of the total area. This may be lower than 33% because part of the metallic nanotubes could have grown on the surface and not reached thermal equilibrium. If we assume that the probability of growing metallic nanotubes is 33%, that would mean that only 63% of the nanotubes have the freedom to reach equilibrium. Significantly, from the standard deviation ( $10.4 \text{ deg}$ ), based on eq 6, we can extract an experimental value for the polarizability of the oriented nanotubes,  $\alpha_{zz} = 4 \times 10^5 \text{ \AA}^2$ , which could be at most five times higher or lower, due to the dispersion of lengths and diameters. The calculated polarizability for metallic nanotubes by eq 4 is  $\alpha_{zz}^M = 2 \times 10^5 \text{ \AA}^2$ , which could be at most four times higher

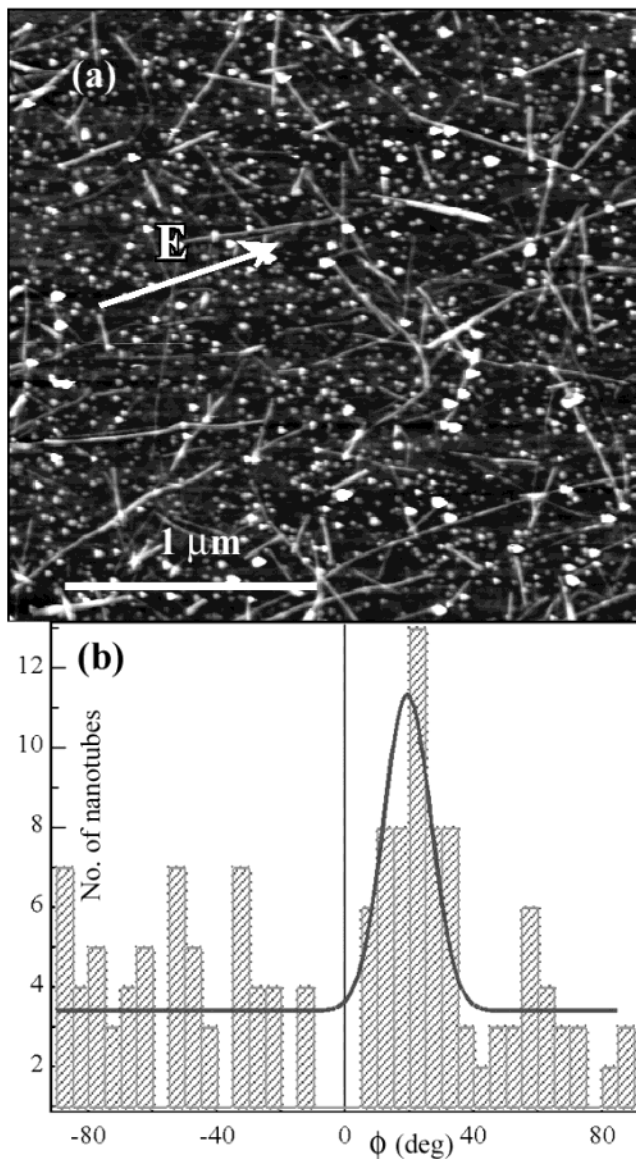


**Figure 3.** (a) Selective field-directed growth of metallic short SWNTs from densely adsorbed ferritin. The AFM image shows a predominant population of SWNTs aligned parallel to the electric field. (b) Histogram representing the corresponding angular distribution of (a) relative to the angle of AFM scanning, which is 20 deg off from the direction of the electric field. Overlaid is a least-squares fitting to Gaussian plus a constant. The optimized Gaussian is centered at 19.5 deg, with a standard deviation of 10.4 deg. The area between the Gaussian and the constant is 21% of the total area below the curve. The applied voltage was 50 V ( $2 \times 10^6$  V/m) and the growth time was 5 min.

or lower, due to the dispersion of lengths. The calculated polarizability for semiconducting nanotubes of similar diameters, according to eq 3, however, is  $1.1 \times 10^2 \text{ \AA}^2$ , which could be at most twice higher or smaller, due to the dispersion of diameters. Thus, the experimental polarizability obtained from the angular distribution is in very good agreement with the calculated value for metallic nanotubes. Although the divergence between the experimental polarizability and the calculated polarizability for metallic nanotubes could be up to 1 order of magnitude, due to the dispersion of diameters and lengths, the calculated value for the polarizability of semiconducting nanotubes of similar dimen-

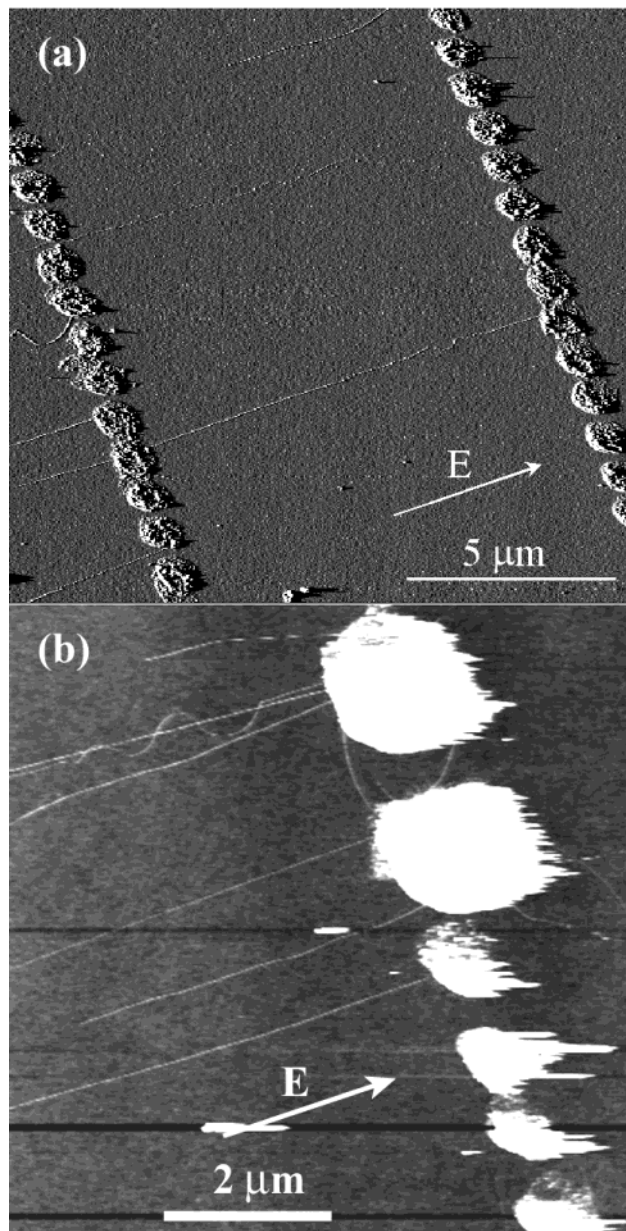


**Figure 4.** (a) Vectorial growth of very long SWNTs ( $L = 10\text{--}15 \mu\text{m}$ ) from ferritin adsorbed on patterned islands of  $\text{Al}_2\text{O}_3$ . Voltage: 50 V ( $2 \times 10^6$  V/m); growth time: 20 min. (b) Vectorial growth of SWNTs from ferritin adsorbed on patterned  $\text{Al}_2\text{O}_3$  islands of different sizes, showing higher densities of parallel SWNTs. The conditions are similar to those in (a).

sions is 3 orders of magnitude smaller than the experimental value. These findings together constitute a strong indication that in the short-nanotube regime, field-directed growth is selective for metallic vs semiconducting nanotubes. Thus, field-directed growth could provide a means of discriminating between metallic and semiconducting single-wall carbon nanotubes during their formation.

Last, vectorial growth of long carbon nanotubes can be achieved by patterning the catalyst by electron-beam lithography, as shown in Figure 4a. These nanotubes are very long ( $>15 \mu\text{m}$ ) and well aligned with the electric field. The nanotube length is essentially limited by the separation between the electrodes ( $25 \mu\text{m}$ ). The yield of nanotubes grown per island can be increased by patterning the catalyst

in larger islands, as shown in Figure 4b, but then the space-resolution of vectorial growth is lower. Better yield and resolution will require further catalyst optimization. A catalyst with 100% yield of nanotube growth should allow a resolution of vectorial growth only limited by the size of the catalyst nanoparticles and the patterning method.

To conclude, we have shown that vectorial growth of SWNTs can be achieved by field-directed growth from patterned catalyst nanoparticles. We have also provided a theoretical analysis and experimental data strongly supporting the hypothesis that field-directed growth can discriminate between metallic and semiconducting nanotubes during their formation. This selectivity remains to be demonstrated by a direct characterization of the electronic type of the nanotubes lying on the surface correlated to their length and their direction with respect to the electric field during growth. Such characterization could, in principle, be done by single-nanotube<sup>27</sup> and polarized<sup>28,29</sup> resonant Raman scattering experiments, and by single nanotube electrical transport measurements. Research along these lines is underway.

**Acknowledgment.** We thank T. Rueckes, K. Kim, C. L. Cheung, J. H. Hafner, and Y. Oreg for helpful discussions. This research was supported by Grant No. 2000218 from the United States–Israel Binational Science Foundation (BSF), Jerusalem, Israel. C.M.L. acknowledges support for this work by the Defense Advanced Research Projects Agency (DARPA) and the Office of Naval Research (ONR).

**Supporting Information Available:** Additional AFM image showing SWNTs grown by the surface growth and free growth mechanisms, from ferrihydrite nanoparticles of different sizes. This material is available free of charge via the Internet at <http://pubs.acs.org>.

## References

- Dresselhaus, M. S.; Dresselhaus, G.; Eklund, P. C. *Science of Fullerenes and Carbon Nanotubes*; Academic Press: San Diego, CA, 1996.
- Dekker, C. *Phys. Today* **1999**, 52, 22.
- Hu, J.; Odom, T. W.; Lieber, C. M. *Acc. Chem. Res.* **1999**, 32, 435.
- Rueckes, T.; Kim, K.; Joselevich, E.; Tseng, G. Y.; Cheung, C. L.; Lieber, C. M. *Science* **2000**, 289, 94.
- Collins, P. G.; Arnold, M. S.; Avouris, Ph. *Science* **2001**, 292, 706.
- Derycke, V.; Martel, R.; Appenzeller, J.; Avouris, Ph. *Nano Lett.* **2001**, 1, 453.
- Bachtold, A.; Hadley, P.; Nakanishi, T.; Dekker, C. *Science* **2001**, 294, 1317.
- Liu, J.; Casavant, M. J.; Cox, M.; Walters, D. A.; Boul, P.; Lu, W.; Rimberg, A. J.; Smith, K. A.; Colbert, D. T.; Smalley, R. E. *Chem. Phys. Lett.* **1999**, 303, 125.
- Diehl, M. R.; Yaliraki, S. N.; Beckman, R. A.; Barahona, M.; Heath, J. R. *Angew. Chem., Int. Ed. Engl.* **2001**, 41, 353.
- Cassell, A.; Franklin, N.; Tomblor, T.; Chan, E.; Han, J.; Dai, H. *J. Am. Chem. Soc.* **1999**, 121, 7975.
- Dai, H. J.; Kong, J.; Zhou, C.; Franklyn, N.; Tomblor, T.; Cassell, A.; Fan, S.; Chapline, M. *J. Phys. Chem. B* **1999**, 103, 11246.
- Franklyn, N. R.; Dai, H. *Adv. Mater.* **2000**, 12, 890.
- Zhang, Y. G.; Chang, A. L.; Cao, J.; Wang, Q.; Kim, W.; Li, Y. M.; Moris, N.; Yenilmez, E.; Kong, J.; Dai, H. *J. Appl. Phys. Lett.* **2001**, 79, 3153.
- Su, M.; Li, Y.; Maynor, B.; Buldum, A.; Lu, J. P.; Liu, J. *J. Phys. Chem. B* **2000**, 104, 6505.
- Kong, J.; Soh, H. T.; Cassel, A. M.; Quate, C. F.; Dai, H. *Nature* **1998**, 395, 878.
- SWNTs were grown by CVD on oxidized silicon substrates containing different iron oxide catalysts, while applying a local electric field parallel to the surface. Silicon wafers (Silicon Sense, Inc.) were degenerately boron-doped and covered with a 600 nm thick insulating thermal oxide layer. The electric field was created over the silicon wafer by a pair of parallel microelectrodes, 10  $\mu\text{m}$  wide, separated by 25  $\mu\text{m}$ , which were fabricated on top of the silicon oxide layer by standard photolithography, successive electron-beam evaporation of  $\text{Al}_2\text{O}_3$  (20 nm), Ti (20 nm), and Pt (60 nm), followed by lift-off. The catalyst was either deposited over the whole silicon oxide surface or patterned between the electrodes by electron-beam lithography, as indicated. The electrodes were wire-bonded with a Pt wire to Pt foil leads on a homemade ceramic chip carrier, which was then placed in a tube furnace and connected by Mo wires through electrical feedthroughs to a power supply electrometer (Keithley 6517). In a typical experiment, the furnace temperature was raised to 800  $^\circ\text{C}$  while flowing 600  $\text{cm}^3/\text{min}$  of Ar and 400  $\text{cm}^3/\text{min}$  of  $\text{H}_2$  through a quartz tube. After this, a typical voltage of 100 or 50 V was applied between the electrodes, as indicated, and ethylene ( $\text{C}_2\text{H}_4$ ) was added at 0.2  $\text{cm}^3/\text{min}$  for a determined period of time. After the reaction, the ethylene and hydrogen flow was stopped, the voltage was switched off, and finally, the furnace was cooled under an Ar flow of 1000  $\text{cm}^3/\text{min}$ . The electrodes were placed parallel to the gas flow, to rule out any possible influence of the flow on the direction of nanotube growth. While applying the voltage, the resistance was monitored and ensured to be always within a range of 1–10  $\text{M}\Omega$ , to avoid accidental electrical leakages, breakdowns, or disconnections.
- The iron oxide catalyst for SWNT growth was prepared and deposited as follows. Iron oxide nanoparticles were either prepared as a cationic ferrihydrite colloid or obtained from the iron-storage protein ferritin, from horse spleen (Sigma), as indicated. Ferrihydrite was prepared<sup>18</sup> by dissolving 2.02 g of  $\text{Fe}(\text{NO}_3)_3 \cdot 9\text{H}_2\text{O}$  in 100 mL of deionized water, adding 0.840 g of  $\text{NaHCO}_3$  while vigorously stirring, and aging for 24 h. Silicon substrates were dipped in a 5-times diluted solution of this sol for 10 min, rinsed in ethanol, and blow-dried. For the random deposition of ferritin, silicon substrates were first activated by dipping in a 0.01% w/w solution of poly-L-lysine for 5 min, rinsed in water, and blow-dried, then dipped in a 1 mg/L ferritin solution, rinsed with water, and blow-dried. These substrates were then oxidized in oxygen plasma, to leave the iron oxide cores of ferritin free of organic matter. Patterning of ferritin between the electrodes was done by a standard electron-beam lithography procedure using poly(methyl methacrylate) (PMMA) as resist. When patterning in long stripes, ferritin was deposited on the exposed silicon oxide areas similarly as described for the random deposition. For patterning ferritin in small islands, a thin  $\text{Al}_2\text{O}_3$  layer (5 nm) was evaporated on the silicon oxide areas exposed through the PMMA, the substrates were dipped in a 1 mg/L ferritin solution, rinsed with water, and blow-dried, then the PMMA was lifted off in 1,2-dichloroethane, and the substrates were cleaned in oxygen plasma. Nanoparticle sizes were determined by atomic force microscopy (AFM).
- Murphy, P. J.; Posner, A. M.; Quirk, J. P. *Aust. J. Soil Res.* **1975**, 13, 189.
- Scanning electron microscopy (SEM) images were obtained with a field-emission SEM (LEO 982), operated at 1 kV with an in-lens detector.
- Benedict, L. X.; Louie, S. G.; Cohen, M. L. *Phys. Rev. B* **1995**, 52, 8541.
- Ouyang, M.; Huang, J.-L.; Cheung, C. L.; Lieber, C. M. *Science* **2001**, 292, 702.
- Odom, T. W.; Huang, J.-L.; Kim, P.; Lieber, C. L. *J. Phys. Chem. B* **2000**, 104, 2794.
- Landau, L. D.; Lifshitz, E. M.; Pitaevskii, L. P. *Electrodynamics of Continuous Media*; Pergamon: Oxford, U.K., 1981.
- Charlier, J.-C.; DeVita, A.; Blasé, X.; Car, R. *Science* **1997**, 275, 646.
- Kanzow, H.; Ding, A. *Phys. Rev. B* **1999**, 60, 11180.
- AFM topographic images were acquired in tapping mode with a Nanoscope IIIa (Digital Instruments, Santa Barbara, CA), using nominal 70 kHz silicon probes.
- Jorio, A.; Saito, R.; Hafner, J. H.; Lieber, C. M.; Dresselhaus, G.; Dresselhaus, M. S. *Phys. Rev. Lett.* **2001**, 86, 1118.
- Jorio, A.; Dresselhaus, G.; Dresselhaus, M. S.; Souza, M.; Dantas, M. S. S.; Pimenta, M. A.; Rao, A. M.; Saito, R.; Liu, C.; Cheng, H. M. *Phys. Rev. Lett.* **2000**, 85, 2617.
- Fantini, C.; Pimenta, M. A.; Dantas, M. S. S.; Ugarte, D.; Rao, A. M.; Jorio, A.; Dresselhaus, G.; Dresselhaus, M. S. *Phys. Rev. B* **2001**, 6316, 1405.

NL025642U